Geophys. J. Int. (1990) **100,** 441–453

Spectroscopic analysis of global tide gauge sea level data

A. Trupin[1] and J. Wahr[2]

[1] *Department of Physics, University of Colorado, Boulder, CO* 80309, *USA*
[2] *Cooperative Institute for Research in Environmental Sciences, University of Colorado, Boulder, CO* 80309, *USA*

Accepted 1989 September 18. Received 1989 September 12; in original form 1989 March 27

SUMMARY

Yearly and monthly tide gauge sea level data from around the globe are fitted to numerically generated tidal data to search for the 18.6-yr lunar nodal tide and 14-month pole tide. Both tides are clearly evident in the results, with amplitudes and phases that are consistent with a global equilibrium response. Global atmospheric pressure data are fitted to global, monthly sea level data to study the response of the ocean to pressure fluctuations. The global response of sea level to pressure is found to be inverted barometer at periods greater than 2 months.

A large coherence at 437 days between pressure and sea level data is found for the north Sea, Baltic Sea and the Gulf of Bothnia. The results are not entirely conclusive, but they tend to support O'Connor's (1986) suggestion that the apparent enhanced pole tide in these basins may be due to meteorological forcing rather than to a basin-scale resonance.

Finally, global averages of tide gauge data, after correcting for the effects of post glacial rebound on individual station records, reveal an increase in sea level over the last 80 yr of between 1.1 and 1.9 mm yr^{-1}. As part of the process of removing the effects of post-glacial rebound, we fit those effects to the global tide gauge data and obtain very good agreement with results predicted from post-glacial rebound models. This tends to support the post-glacial model results and it suggests that the global tide gauge data are, indeed, capable of resolving changes in sea level at the mm yr^{-1} level.

Key words: pressure, sea level, stacking, tides.

INTRODUCTION

Long-period ocean tides affect estimates of certain geophysical parameters, in some cases through oceanic contributions to the Earth's inertia tensor and, in others, through crustal deformation caused by the tidal loading. Two examples of such estimates are the use of satellite solutions for the earth's J_2 gravity coefficient to constrain mantle anelasticity at the lunar tidal period of 18.6 yr, and the use of the observed period and damping of the Chandler wobble to estimate anelasticity at the 14-month wobble period.

The 18.6-yr solid-Earth and ocean tides, related to the precession of the lunar nodes, cause an 18.6-yr variation in J_2. Lambeck and Nakiboglu (1983) assumed the ocean tide was equilibrium (for an 'equilibrium' tide, the sea surface is a surface of constant potential) and used Rubincam's (1984) observed 18.6-yr variability in J_2 to constrain the value of mantle anelasticity at this period. The result was surprisingly large. To help assess the importance of the equilibrium ocean tide assumption on the conclusion, we note that if the Earth were assumed to be elastic, Rubincam's (1984) result would imply an 18.6-yr ocean tide that was twice equilibrium. The J_2 result should continue to improve as more satellite data are acquired.

The Chandler wobble constraint on anelasticity (see, for example, Smith & Dahlen 1981) depends critically on the response of the ocean to the incremental centrifugal force caused by the wobble. That response, called the pole tide, is known to affect the period and, if it were non-equilibrium, could contribute to the damping. In fact, a global departure from equilibrium of only 10 per cent could have observable consequences. Theoretical models for the pole tide in the deep ocean suggest the pole tide should be equilibrium (O'Connor & Starr 1983; Carton & Wahr 1986; Dickman 1988a). However, the pole tide in the North and Baltic Seas and in the Gulf of Bothnia is apparently several times the equilibrium value (Miller & Wunsch 1973). Wunsch (1986) postulated that this enhanced tide may be due to a local oceanic resonance in the region. Alternatively, O'Connor

(1986) suggested that the apparent 14-month spectral peak could be caused by meteorological forcing and is not related to the pole tide.

The response of the ocean to variations in atmospheric pressure is another oceanographic disturbance with implications for solid earth geophysics. An inverted barometer response (i.e. a 10-mm depression of sea level for every 1-mbar increase in pressure) is suggested by analytical models (see e.g. Wunsch 1972; Munk & MacDonald 1975; Dickman 1988b). The inverted barometer assumption has been invoked when studying the effects of atmospheric pressure on the Earth's rotation (see e.g. Munk & Hassan 1961; Wilson & Haubrich 1976; Merriam 1982; Wahr 1983) and when estimating the crustal deformation caused by pressure fluctuations (Rabbel & Zschau 1985; Van Dam & Wahr 1987). The results in both cases are sensitive to the accuracy of this assumption. It is also important to understand the pressure response in order to interpret observed sea level variability in terms of wind-driven ocean currents. For example, oceanographers who process altimeter data to learn about the wind-driven response usually remove an inverted barometer pressure response during data pre-processing.

Climate models that are used to study the effects of atmospheric greenhouse gasses predict an increase in the global temperature over the next century of from 1° to 4 °C (Hansen *et al.* 1981). An increase of this magnitude could have numerous catastrophic effects, not the least of which would be a global rise in sea level due to a combination of melting polar ice caps and the thermal expansion of sea water. One of the important goals of global change studies is to improve our understanding of this variability in water storage.

There have been previous attempts to use tide gauge data to constrain the 18.6-yr and 14-month tides (see e.g. Munk & Cartwright 1966; Cartwright & Tayler 1971; Miller & Wunsch 1973; Hosoyama, Naito & Sato 1976) the response of the ocean to atmospheric pressure (Chelton & Enfield 1986) and the global rise in sea level (Emery 1980; Gornitz, Lebedeff & Hansen 1982; Barnett 1983; Peltier 1986). These studies have primarily involved the analysis of data from individual tide gauges or, at most, from a small subset of all available stations.

In the present study, we combine tide gauge data from several hundred stations scattered around the globe, to test the hypotheses that the global 18.6-yr and 14-month tides are equilibrium, and that the response to pressure is inverted barometer. Our tide gauge data set consists of monthly sea level values obtained from the Permanent Service for Mean Sea-Level (PSMSL), at Bidston, England (see Pugh & Faull 1983a). The distribution of the 721 stations over the globe is shown in Pugh & Faull (1983b). In all cases, our observational results are consistent with these hypotheses (although the time resolution of the data limits the investigation of the pressure-driven response to forcing periods of greater than 2 months).

We investigate the possible causes of the apparently enhanced pole tide in the North Sea region. Our comparisons between tide gauge and pressure data tend to support the hypothesis that the spectral peak is due to narrow-band meteorological forcing in the region, rather than to a basin-scale resonance. Our conclusions, though, should be regarded as tentative, because the dominant meteorological forcing would be due to winds, but we did not include wind data in our analysis.

We also use the PSMSL data to constrain the global rise in sea level. Although our estimates vary somewhat, depending on how we restrict the data and correct for post glacial rebound (see e.g. Peltier 1986) we infer a global sea level rise of between 1.1 and 1.9 mm yr^{-1}, with a preferred value of 1.75 mm yr^{-1} for stations in the regions covered by Peltier's (1986) model. In the process of correcting for the effects of post glacial rebound, we least-squares fit Peltier's (1986) predicted vertical uplift to the data, and find very good agreement (i.e. a fit with a value close to 1).

METHODS OF ANALYSIS

In this section, we describe two methods we use to help identify small signals in the global tide gauge data. We use the least-squares fit technique to study the ocean's response to atmospheric pressure. Also, we stack the data to investigate the 18.6-yr tide and the 14-month tide. We use both techniques to study the global rise in sea level and the effects of post glacial rebound. We use the monthly PSMSL data to study the pole tide and the response to atmospheric pressure. We use yearly averages of the PSMSL data to study the 18.6-year tide and the global rise in sea level.

Least-squares fit

Let $s_k(t)$ and $p_k(t)$ represent the time-dependent fluctuations in sea level and in pressure at tide gauge k. Separate the observed sea level fluctuations into a component caused by the pressure, and a remainder, $\varepsilon_k(t)$, due to a combination of wind-driven fluctuations, tides, and observational noise. Suppose that the pressure-induced variability at an individual tide gauge depends on the past, present, and future values of pressure as measured at that gauge alone. (Except in cases where the arrival of pressure-driven waves precedes the arrival of the change in pressure, causality precludes dependence on the future, but by solving for that dependence we can partially assess the accuracy of our results.) Then, the most general linear relationship between s_k and p_k is

$$s_k(t) = \int_{-\infty}^{\infty} A(\tau) p_k(t-\tau)\, d\tau + \varepsilon_k(t). \tag{1}$$

Here, $A(\tau)$ can be interpreted physically as a Green's function describing the response of the ocean to an impulsive pressure disturbance (the true Green's function would actually be more complicated than $A(\tau)$, since equation (1) assumes that sea level at any point is unaffected by pressure disturbances at other points). Since the ocean has a finite memory, $A(\tau)$ should approach zero for large τ.

Suppose that both $s_k(t)$ and $p_k(t)$ are discretized to a time series of monthly values, $t = t_i$, and suppose $A(\tau)$ is negligible for $|\tau| > Lt_i$, where L is an integer. If Δt is the sampling interval (equal to 1 month in our case), then (1) reduces to the discrete form

$$s_k(t_j) = \sum_{i=-L}^{L} A(t_i) p_k(t_j - t_i)\, \Delta t + \varepsilon_k(t_j). \tag{2}$$

For an inverted barometer ocean, $A(0)$ would be $-10.1\,\text{mm mbar}^{-1}$ (see Wunsch 1972), and all other $A(t_i)$ would be zero.

Suppose $A(t_i)$ is independent of the tide gauge location. This is equivalent to assuming that the ocean responds to pressure in the same way at every location. Then, we can estimate $A(t_i)$ for each t_i by least-squares fitting to all PSMSL tide gauge data simultaneously. We can least-squares fit each $A(t_i)$ individually, or all the $A(t_i)$ simultaneously. As an example, if each data point is given equal weight, regardless of where or when it was taken, and if M_k is the total number of months in the time series for tide gauge k, then the least-squares fit for an individual $A(t_i)$ gives

$$A(t_i) = \frac{\sum_{k=\text{gauge}} \sum_{j=1}^{M_k} s_k(t_j) p_k(t_j - t_i)}{\sum_{k=\text{gauge}} \sum_{j=1}^{M_k} p_k(t_j - t_i) p_k(t_j - t_i)}. \quad (3)$$

As another application, the PSMSL data are simultaneously fit to theoretically predicted post-glacial rebound data and to a global linear trend, to estimate the global rise in sea level and to help assess the rebound models. The rebound data are constructed from the linear trends predicted for each station by the models, and are identical to the PSMSL data in coverage and gaps. Whereas the effects of ice melting and thermal expansion on sea level is assumed here to be independent of position, the linear trends due to post-glacial rebound are not. To the extent the rebound varies with position, it may be separated from the general increase in sea level by the simultaneous fit. The fit to the rebound model gives information on which stations should be included in the simultaneous fit, as described below. It also allows us to partially assess the accuracy of the rebound models, and of the global sea level rise inferred from the tide gauge data.

Stacking

The procedure of stacking multistation data to enhance small signals has been used by seismologists to improve their estimates of the Earth's free oscillation eigenfrequencies (Gilbert & Dziewonski 1975), and to search for short-period oceanic normal modes in the Pacific (Luther 1982). Stacking is particularly useful in cases where the spatial dependence of the signal is known beforehand.

Suppose we want to test the hypothesis that the 18.6-yr tide is equilibrium. The 18.6-yr equilibrium amplitude at colatitude θ, eastward longitude λ, and time t, has the form [using the corrected tables of tidal harmonics from Cartwright & Edden (1973)]

$$H(t, \theta, \lambda) = 27.94\zeta(\theta, \lambda)\cos(\omega t + \phi) \quad \text{mm} \quad (4)$$

where ω is the frequency of the 18.6-yr tide and ϕ is the phase at $t = 0$. The function $\zeta(\theta, \lambda)$ represents the spatial dependence of the equilibrium tide, and would equal $(1 + k - h)Y_2^0$ *were it not for mass conservation of the oceans, sea-floor loading, and gravitational self attraction (h and k are tidal Love numbers, and the spherical harmonic* Y_2^0 *is normalized so that the integral over the unit sphere of* $|Y_2^0|^2$ *is one). These latter effects cause the introduction of* other spherical harmonics into $\zeta(\theta, \lambda)$ and increase the Y_2^0 component by about 10 per cent. The function $\zeta(\theta, \lambda)$ can be found by iterative solution of equation (102) in Dahlen (1976).

Once we have found $\zeta(\theta, \lambda)$, we least-squares fit it to all the PSMSL tide gauge data at each time t (see equation 6, below). The average and the secular trend are removed from each station prior to the fit. The resulting time series of fit values is referred to here as a stack. The stack is spectrally analysed to search for a peak at the 18.6-yr frequency, ω. If a peak is found, its amplitude and phase can be compared with the results that would be expected for an equilibrium tide. To estimate these equilibrium results, a synthetic data set is constructed by replacing the PSMSL sea level value at every gauge and at every time by the estimated equilibrium value, $h(t, \theta, \lambda)$ in (4), at that same position and time. The synthetic data, like the PSMSL data, are stacked against the equilibrium spatial dependence $\zeta(\theta, \lambda)$ and the amplitude and phase of the spectral peak at 18.6 yr are estimated.

Good agreement between these stacks of PSMSL and synthetic data is not enough to guarantee that the tide is equilibrium. It is desirable to also stack against other functions of θ and λ. For example, the equilibrium $\zeta(\theta, \lambda)$ for the 18.6-yr tide is nearly proportional to $Y_2^0(\theta, \lambda)$. We stack against other spherical harmonics as well, up to degree 6. These additional stacks serve two purposes. First, by stacking the synthetic data we can assess the effectiveness of the stacking procedure. For instance, is the station coverage complete enough that different spherical harmonics are reasonably orthogonal? We find that it is. Second, by stacking the PSMSL data and looking at the spectra, we can further test the equilibrium assumption. For example, if the data are stacked against a spherical harmonic other than Y_2^0, and if the 18.6-yr tide is equilibrium, then there should not be a notable peak at 18.6 yr in the spectrum of the stack. Although we do not show results here for these other stacks, we find no evidence of 18.6-yr peaks that stand significantly above the noise continuum for any stacks against pure spherical harmonics other than Y_2^0. We compare these PSMSL results with Y_l^m stacks of the synthetic data, and find that the 18.6-yr peaks in the synthetic stacks are also below the noise continuum of the PSMSL spectra. These results, then, are consistent with the equilibrium hypothesis. That hypothesis is addressed further, below, when we discuss the stacks against the equilibrium $\zeta(\theta, \lambda)$.

A similar procedure is used to investigate the 14-month pole tide. The equilibrium pole tide is generated from polar motion data [we use polar motion values from the International Latitude Observatory of Mizusawa; see Yumi & Yokoyama (1980)] according to

$$H(t, \theta, \lambda) = \frac{-3\Omega^2 a^2}{2g} \mathcal{R}e\{[m_1(t) + im_2(t)]\zeta(\theta, \lambda)\}. \quad (5)$$

Here, $m_1(t)$ and $m_2(t)$ are the $\hat{\mathbf{x}}$ and $\hat{\mathbf{y}}$ coordinates of the pole position (with magnitude up to one third of an arcsecond), Ω and a are the Earth's mean rotation rate and radius, and $\mathcal{R}e$ denotes the real part. The spatial dependence, $\zeta(\theta, \lambda)$, in (5) is complex, and so when it is least-squares fit to the PSMSL data it gives a complex stack. In the absence of sea-floor loading, gravitational self

attraction, and mass conservation, $\zeta(\theta, \lambda)$ would equal $(1+k-h)Y_2^1(\theta, \lambda)$. As in the case of the 18.6-yr tide, $\zeta(\theta, \lambda)$ is modified by about 10 per cent due to these additional effects, and it can be estimated as described by Dahlen (1976). Stacks against the equilibrium $\zeta(\theta, \lambda)$ are described below. Stacks of the PSMSL data against spherical harmonics other than Y_2^1 do not exhibit significant peaks at the 14-month pole tide period, and are consistent with Y_l^m stacks of the synthetic data.

For any of these examples, the least-squares fit to form a stack can either be weighted or unweighted. One weighting procedure we find to be particularly useful involves stacking on a grid. The Earth's surface is divided into grid elements, in our case either 10° latitude by 20° longitude or 15° latitude by 30° longitude. Sea level heights for each station (with secular trends and station averages removed) are multiplied by the equilibrium spatial dependence, $\zeta(\theta, \lambda)$, and the results are averaged over individual grid elements for a given time, t. A global average is then constructed by summing the grid averages. The final result is normalized by dividing by the global average of the equilibrium data. The resulting time series is the weighted stack.

For example, let $s_k(t)$ be the tide gauge reading for station k at time t, with the secular trend and station average removed. Let θ_k and λ_k be the colatitude and eastward longitude of station k. Let $n_p(t)$ be the total number of gauge measurements in grid element p at time t, and suppose there are N grid points. Then, the complex gridded stack, $x(t)$, is defined as

$$x(t) = \frac{\sum_{p=1}^{N} \frac{1}{n_p(t)} \sum_{\substack{k=\text{gauges} \\ \text{in } p}} s_k(t)\zeta(\theta_k, \lambda_k)}{\sum_{p=1}^{N} \frac{1}{n_p(t)} \sum_{\substack{k=\text{gauges} \\ \text{in } p}} \zeta^*(\theta_k, \lambda_k)\zeta(\theta_k, \lambda_k)}. \quad (6)$$

Here * denotes complex conjugation. This result, (6), is equivalent to a weighted least-squares fit of ζ to the data at time t, and it reduces to an ungridded, unweighted stack when the grid elements are so small that $n_p(t) = 1$ for every p.

Individual station records exhibit considerable long-period variability; most of it probably caused by forcing from surface winds. This makes it difficult to use a single tide gauge record to identify any of the long-wavelength spectral features we are considering here. Stacking the individual stations against the spatial dependence of the equilibrium solution amplifies any signal with that spatial dependence, and this can significantly reduce the correlation with the wind-driven variability.

The use of grid de-emphasizes areas with great concentrations of stations, such as northern Europe and Japan, by weighting them equally with areas of fewer stations. Gridding also tends to further reduce the contamination from long-wavelength, wind-driven features. Roughly speaking, the contamination of the final stack is reduced when the wind-driven signal has wavelengths much longer than the grid size, but is increased at shorter wavelengths.

For example, imagine a situation where there are 10 stations: nine within grid element A and one within a far distant grid element B. If the wind-driven signal has a wavelength much longer than the grid size, then within grid element A that signal is highly correlated with the long-wavelength feature we are interested in: both are nearly constant across the element. In that case, an ungridded stack would not effectively remove the wind-driven signal, since the stack would be dominated by the high correlation at the nine stations within A. A gridded stack would be more effective, since then the nine elements in A would be weighted equally with the one element in B, and thus the stack could more effectively exploit any differences between the signals at A and B.

On the other hand, since isolated stations contribute more heavily to a gridded stack, that stack is more sensitive to noise in those individual station records. The sizes of the grids used here are chosen to be large enough to minimize the effects of wind-driven fluctuations and of gaps in the grid averages, but smaller than the wavelength of the dominant spherical harmonic in the stacking function. The yearly data are stacked on a coarser grid than are the monthly data. In each case, the grid size that is selected is the one for which the background noise for the stack is minimized.

Subtracting the average tide gauge height for each station prior to a stack is necessary to establish a uniform benchmark for all stations. But, if a station does not report data over the entire time span of the stack, the computed station average is not the true average, and this can introduce systematic errors into the spectrum. (Of the 721 stations in the PSMSL data set, only seven cover the entire interval between 1900 and 1979.) The frequency content of these errors depends on the time spans of the individual station data. The errors are likely to be important at periods close to and longer than the average of the station lengths. Although we have found no consistent way of eliminating these errors, we have attempted to minimize their impact by only including stations with data spans that are longer than the period of the signal we are looking for (at least when we can define that period). The pole tide results are not particularly sensitive to this problem since the average station length for all PSMSL stations is 29 yr, which is many times the period of the tide.

Fitting and removing secular trends from stations prior to stacking is found to remove another source of error, as power associated with these trends can leak into the spectral band of interest. In addition, before any spectral analysis is performed on the final stacks, a secular trend and an average are removed from the final time series. (Even if trends and averages are removed from the individual station data, there can still be a trend and a non-zero average in the stacked data, if the stack is weighted, because an individual station does not, in general, report data over the entire time span of the stack.)

The spectral methods employed here to analyse a stack include finding conventional amplitude and coherence spectra, and using the more sophisticated multitaper method developed by Thomson (1982) to minimize spectral leakage and adapted for geophysical applications by Lindbergh, Park & Thomson (1987). For the multitaper technique, the data are multiplied by one of six prolate spheroidal sequences, or tapers, to create six time series. A spectrum is then constructed from the discrete Fourier transforms of each of these series following section 3, part 1, of Lindbergh *et al.* (1987). A statistical F-test provides a confidence

estimate that an apparent periodicity in the spectrum is truly sinusoidal.

The conventional amplitude spectra shown here all employ a cosine taper. Following convention, we construct complex Fourier transforms as twice the real transform, and the amplitude spectrum is the absolute value of the complex Fourier transform. All of the amplitude spectra shown in the figures are overresolved. By this, we mean that the absolute amplitude is computed at more frequent intervals than the elementary bandwidths, in order to obtain a clearer idea of where the actual peaks lie. To find the coherence at frequency ω between two time series, the time series are multiplied by a cosine taper, and the average coherence across seven elementary bandwidths centred on ω is calculated according to equation (5) of Wilson & Haubrich (1976). With this choice for the coherence spectrum, we can be 95 per cent confident that two series are correlated at ω, if the coherence at ω is larger than 0.43. Other choices of tapers and bandwidths are possible (see Chao 1988).

RESULTS

The response to pressure

Figure 1 shows a plot of the least-squares fit parameter, $A(\tau)$ [equation (3) with $t_i = \tau$], between sea level and atmospheric pressure, for lag times of up to ±240 months. The pressure data are obtained from an objective analysis of global station pressure data for January 1900–April 1973 (Wahr 1983), and so we restrict the PSMSL data to this time period. Seasonal effects are removed from both sea level and pressure data sets prior to the fit.

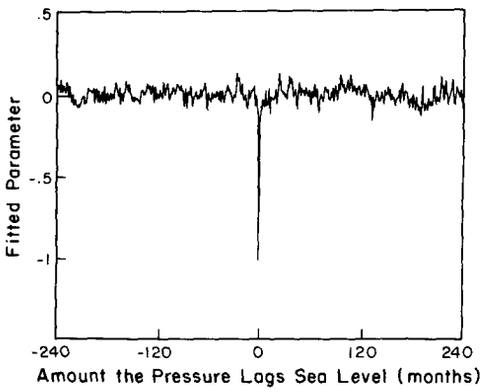

Figure 1. The coefficients, $A(\tau)$, of the least-squares fit of sea level to atmospheric pressure for 487 stations outside the North and Baltic Seas and Gulf of Bothnia. Seasonal averages have been removed from both the pressure and sea level data. The response is consistent with the inverted barometer assumption for time lags of up to ±240 months.

All PSMSL stations during this time period are included in the fit shown in Fig. 1, except for those in the North and Baltic Seas and in the Gulf of Bothnia. As shown below, the Baltic Sea and Gulf of Bothnia do not appear to be inverted barometer (although the North Sea does). Furthermore, by omitting these three shallow seas from the data, we end up using the same data subset in Fig. 1 that we will use later to study the global pole tide.

The result for $A(0)$ is $-10.1\,\mathrm{mm\,mbar^{-1}}$ for the fit shown in Fig. 1. The results for all other $A(\tau)$ are close to zero, with an rms value of $0.5\,\mathrm{mm\,mbar^{-1}}$. Consequently, we assign $\pm 0.5\,\mathrm{mm\,mbar^{-1}}$ to be the uncertainty in our estimate of $A(0)$. Since wind data were not analysed, there is no way for us to separate the contribution of winds to the fit to pressure. There should be a temporal correlation between winds and pressure at each tide gauge. Our hope is that there are enough stations over a wide enough area in the global average to break the spatial correlation between winds and pressure. Without wind data we cannot confirm that this has happened, but the results shown in Fig. 1 are at least consistent with an inverted barometer response of the oceans to pressure at periods of 2 months and longer.

The response for zero lag for other sets of stations is given in Table 1. In all these fits, the $A(\tau)$ for $\tau \neq 0$ are close to zero. The rms values for these other $A(\tau)$ are shown as the uncertainties for $A(0)$. Note that as the number of stations included in the fit decreases, the rms value for $A(\tau)$ with $\tau \neq 0$ increases.

These results include examples of shallow basins where the deviation from the inverted barometer response for $A(0)$ exceeds the rms value of the other $A(\tau)$s. This does not necessarily imply a true non-inverted barometer response, because the rms value does not adequately represent everything that could bias the fit. In particular, wind-driven changes in sea level could be correlated with surface pressure, and thus could affect our estimate of $A(0)$ without contributing noticeably to $A(\tau)$ for $\tau \neq 0$. This is apt to be a particular problem when considering small regions at a time, such as the Baltic Sea and the Gulf of Bothnia, since then there is likely to be greater spatial coherence between the wind and pressure fields.

The pole tide

Monthly tide gauge data are stacked, as described above, to study the pole tide. Before stacking the data, we remove the

Table 1. The response for zero lag for various sets of stations.

Set of stations	$A(0)$ ($\mathrm{mm\,mbar^{-1}}$)	No. stations
Global oceans including all shallow basins	-12.1 ± 0.9	574
Northern hemisphere excluding North Sea region	-10.0 ± 0.5	407
Eastern hemisphere excluding North Sea region	-10.3 ± 0.7	234
Southern hemisphere	-10.9 ± 1.1	80
Western hemisphere	-9.9 ± 0.6	253
North Sea	-9.7 ± 0.9	26
Baltic Sea	-12.5 ± 1.3	42
Gulf of Bothnia	-16.2 ± 1.7	19
Mediterranean Sea	-14.4 ± 1.2	33

effects of atmospheric pressure, computed using the inverted barometer assumption. Again, we restrict our analysis to January 1900–April 1973. We find that, for stations outside the North Sea, Baltic Sea, and Gulf of Bothnia, the removal of pressure affects the pole tide amplitude inferred below by about 10 per cent.

In this and the succeeding analysis involving the pole tide, stations in the North and Baltic Seas and in the Gulf of Bothnia are removed from the PSMSL data as there is an anomalously large spectral peak at 434–437 days for this region close to the pole tide peak at 437 days (see, for example, Miller & Wunsch 1973). An equilibrium stack of 26 stations in the North Sea reveals the PSMSL amplitude at the 437-day period to be 3.6 times the equilibrium amplitude, for the 42 Baltic Sea stations the PSMSL amplitude is 6.2 times equilibrium, and for the 19 stations in the Gulf of Bothnia, the PSMSL amplitude exceeds the equilibrium amplitude by a factor of 9.

The beat period between the pole tide band and one year is approximately 60–85 months. To minimize the correlation with the annual period, we choose to include in our global analysis only those stations having greater than 60 months of data. This leaves us with 487 stations out of the original 721 in the full PSMSL data set.

Figure 2(a) shows ungridded amplitude spectra for Y_2^1 stacks of these 487 stations. Fig. 2(b) shows the spectra of the stacks averaged on a $10° \times 20°$ grid. Shown are the spectra for the PSMSL data, for the synthetic (i.e. equilibrium) data, and for differenced data. The differenced data are generated by subtracting the synthetic time series from the PSMSL time series. Note that in Fig. 2 the spectra for both the PSMSL data and the synthetic data show a double peak for the pole tide, with one peak at 427 days and the other at 437 days. This is a well-known feature of the polar motion spectrum. Most of the signal contributing to this double peak is from data early in the time series. The two peaks are close enough together that their resolution requires most of the 74 yr of the data span.

In both the gridded and non-gridded stacks, the pole tide is clearly evident in the spectrum for the PSMSL data and there is good visual agreement with the synthetic data. The agreement is particularly good for the gridded results. In both cases, the differenced data does not have the characteristic double peak spectrum, indicating that the PSMSL stack is similar to the equilibrium stack in amplitude and phase.

To evaluate the agreement quantitatively, we compute amplitudes for both the PSMSL and the synthetic data sets. First, the amplitudes at the frequencies of the two apparent pole tide peaks are computed, and the results from the PSMSL data and synthetic data are compared. We find, for the ungridded data shown in Fig. 2(a), that the amplitude of the 427-day peak in the PSMSL data is 0.99 ± 0.28 times the synthetic amplitude, and that of the 437-day peak is 0.74 ± 0.27 times the synthetic.

We then repeat this procedure, but for the gridded stacks in Fig. 2(b). In this case, the 427-day and 437-day amplitude ratios are 1.01 ± 0.18 and 0.96 ± 0.17 respectively. The uncertainties for both the gridded and ungridded results are obtained from visual estimates of the signal-to-noise ratio at the pole tide frequency, and assuming the worst case that the amplitudes of the signal and the noise are additive (in other words, that the noise is either in phase or 180° out of phase with the signal). The background amplitude used to obtain the signal-to-noise ratio is 1.0 mm for both the ungridded and gridded stacks.

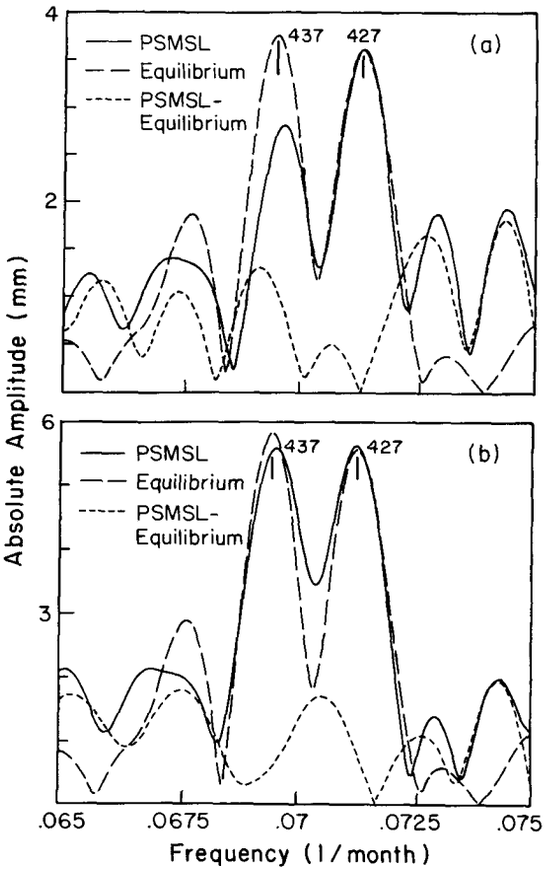

Figure 2. Amplitude spectra at the Chandler wobble frequency band for Y_2^1 stacks of 487 stations. The solid curve is for the PSMSL stack, the long-dashed curve is for the synthetic (equilibrium) data and the short-dashed curve is the spectrum obtained when the synthetic stack is subtracted from the PSMSL stack. The effects of pressure have been subtracted from the PSMSL data, assuming an inverted barometer response. The Chandler wobble is clearly evident in the PSMSL results, and its amplitude is close to equilibrium. Stations in the North and Baltic Seas and in the Gulf of Bothnia are not included in the stacks. (a) Ungridded. (b) $10° \times 20°$ grid.

To estimate the phase difference between the PSMSL and the synthetic data and to obtain another estimate for the amplitude ratio, we fit the synthetic data to the PSMSL data using a complex constant, after a filter is used to extract, from both time series, the power in a spectral band centred over the two pole tide frequencies (0.068–0.073 cycles per month). The power in the spectral band of interest is extracted so that the band at the annual period and the low-frequency power does not affect the estimate of phase (there is a residual spectral peak centred around 1 cycle per year, even though an annual term has been fit and removed from the data). The phase difference between the PSMSL and the synthetic data is small for both the gridded and ungridded stacks. The PSMSL leads the synthetic data in the ungridded stacks by $3° \pm 50°$ and the overall amplitude ratio is 0.83 ± 0.27; roughly the average of the amplitude ratios

taken for each spectral peak separately. For the gridded data the PSMSL leads the synthetic data by $0° \pm 46°$ and the amplitude ratio is 0.96 ± 0.18. A phase lead, δ, is defined here so that if the equilibrium tide is proportional to $\cos(\omega t - \lambda)$, where λ is eastward longitude and ω is the (positive) pole tide frequency, then the observed ocean tide is proportional to $\cos(\omega t - \lambda + \delta)$. Each degree of phase lead represents a time lead of approximately 1.2 days.

To estimate the uncertainty in the phase, we note that the amplitude uncertainty found from the signal-to-noise ratio, as described above, mostly reflects the uncertainty in the in-phase component. We assume the uncertainty in the out-of-phase component is just as large, and compute the resulting bounds on the phase. This procedure results in a larger uncertainty than that predicted from the formal error of the fit.

We have also computed the multitaper spectrum, as described above, for the gridded equilibrium stack. The results do not differ significantly from the conventional spectral results, probably because the cosine taper in the conventional spectra is sufficient to exclude the majority of spectral leakage into the pole tide band.

Taken together, the Y_2^1 stacks of monthly data suggest that the pole tide amplitude is 0.9 ± 0.3 times the equilibrium amplitude, and that the actual ocean tide leads the equilibrium pole tide by $2° \pm 48°$.

The enhanced pole tide in the north seas

Figure 3(a) shows untapered amplitude spectra of surface pressure, PSMSL sea level data, and the equilibrium pole tide stacked against Y_2^1, for the North Sea. The surface pressure results are obtained by multiplying the pressure data described above by the inverted barometer factor of 10.1 mm mbar^{-1}, and then replacing each tide gauge reading with the inverted barometer value at the time and location of that reading. Figs 3(b) and (c) show the same spectra for the Baltic Sea and Gulf of Bothnia respectively. For these small seas, a Y_2^1 stack is not much different than a spatial average. The same spectra are plotted for the 487 stations that span the remainder of the globe in Fig. 3(d). In all the figures, amplitude is shown instead of power to compare the three disparate spectra most clearly. Note that in all three shallow seas, there is a pronounced sea level peak in the pole tide band, that stands well above the equilibrium results.

We have attempted to interpret the 14-month peak in the sea level data in terms both of meteorological forcing (O'Connor 1986) and of a local oceanic resonance (Wunsch 1986). We formulate two hypotheses. One is that there is a resonance that amplifies the response of this region to external forcing. Such a resonance should affect both the pole tide and the response to meteorological forcing. The

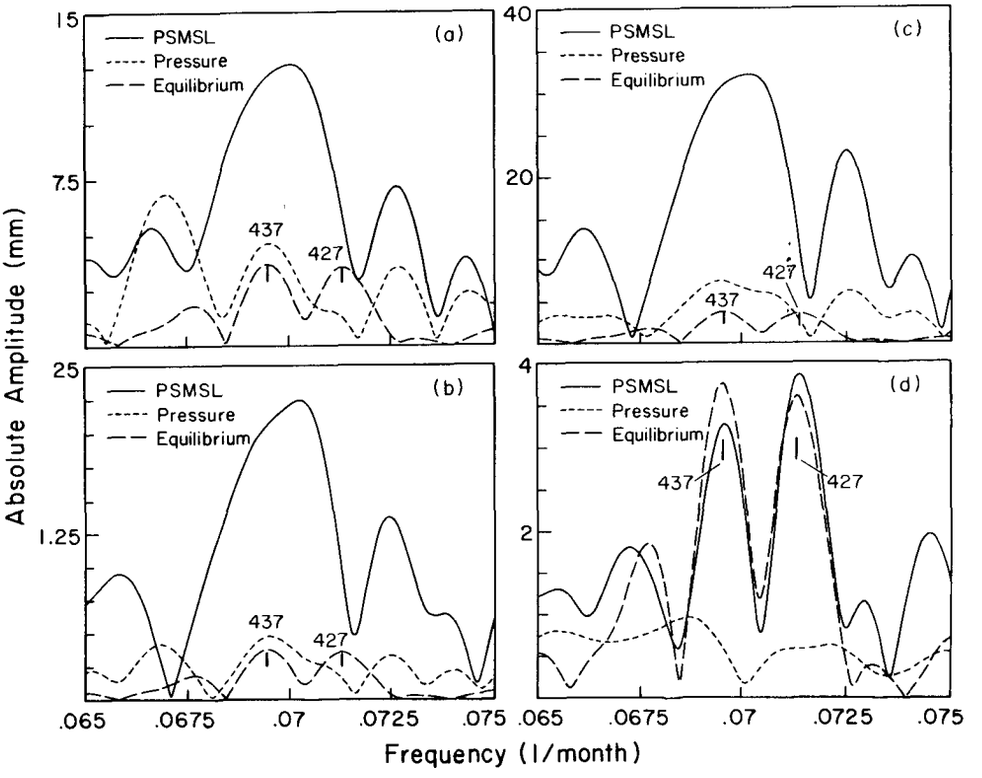

Figure 3. Amplitude spectra of Y_2^1 stacks of sea level, pressure, and the equilibrium pole tide (solid, short-dashed, and long-dashed curves respectively) for: (a) the North Sea (sea level is 3.6 times the equilibrium pole tide at the 437-day period); (b) the Baltic Sea (sea level is 6.2 times equilibrium at the 437-day period); (c) the Gulf of Bothnia (sea level is 9 times equilibrium at the 437-day period); (d) the global oceans outside the North Sea region (the sea level and equilibrium spectra are in good agreement, and there is no prominent pressure peak in the pole tide frequency band). This figure differs from Fig. 2(b) in that, here, seasonal averages have been removed from the PSMSL data but pressure has not. The pressure data have been multiplied by 10 mm mbar^{-1} prior to constructing the stack. Note the similarity between the sea level and pressure spectra for each of the three shallow basins. In this figure and in Fig. 4, the peaks in the pressure and sea level are as narrow as the pole tide band itself.

other hypothesis is that there is no local resonance, but that the spectral peak in sea level is due to a combination of an equilibrium pole tide and a static response to meteorological forcing (i.e. an inverted barometer response to pressure and a response to local winds). We assume that the winds are correlated with the pressure in this frequency band, so that the total stacked response of the ocean to the meteorology is proportional to the stacked pressure data across this frequency band.

To assess these two hypotheses, we first note that for the three shallow basins, there is a pressure peak at the 437-day period, close to coincident with the pole tide period. In fact, the peaks in the sea level spectra appear to line up reasonably well with peaks in the pressure spectra. There seems to be less agreement between the sea level and equilibrium pole tide spectra. On the other hand, for the global results there is good apparent agreement between sea level and the equilibrium pole tide, and less similarity between sea level and pressure.

Coherence results tend to support this observation. Coherence spectra between Y_2^1 stacks of sea level and pressure are shown in Fig. 4(a) for the North Sea, Fig. 4(b) for the Baltic Sea, and Fig. 4(c) for the Gulf of Bothnia. The reason for using stacks against Y_2^1, instead of simple averages, is for consistency with the global results. To minimize spectral leakage from the annual into the pole tide bands, seasonal averages have been removed from all data from which coherence spectra are generated. For all three shallow basins, there is a correlation above the 95 per cent confidence level between sea level and pressure in the frequency band of the pole tide (a coherence estimate greater than 0.43). The coherence is particularly strong over the Gulf of Bothnia. Although there is a 5 per cent chance that the large coherence is spurious, it is interesting that it occurs in a frequency band where there are large amplitude spectral peaks in both pressure and sea level. Fig. 4(d) shows the same coherence spectrum for the Y_2^1 stack of 487 stations outside the North Sea region. There, the correlation between pressure and sea level in the pole tide band is somewhat below the 95 per cent confidence level. (There is a large coherence at a period of about 460 days, just left of the pole tide band.)

Note that for all three shallow seas, there are narrow-band estimates of coherence between sea level and pressure above the 95 per cent confidence level at several frequencies outside the pole tide band. While it is not unusual for the oceans to be stressed by winds and pressure enough to show enhanced coherence at a particular frequency, what is coincidental is the existence of a normal mode of the Earth (the Chandler wobble) near one of the peaks in the local pressure spectrum, and the fact that the meteorological forcing in this case is concentrated in a frequency band that is about as narrow as the pole tide peak.

In order to test for the existence of a high-Q periodic signal in the atmosphere, a statistical F-test was calculated from the Thomson spectrum of the pressure signal for these three regions. In all three regions, the F-test value is greater than the 90 per cent confidence level, suggesting, without any clues as to the cause, that there is a periodic signal in

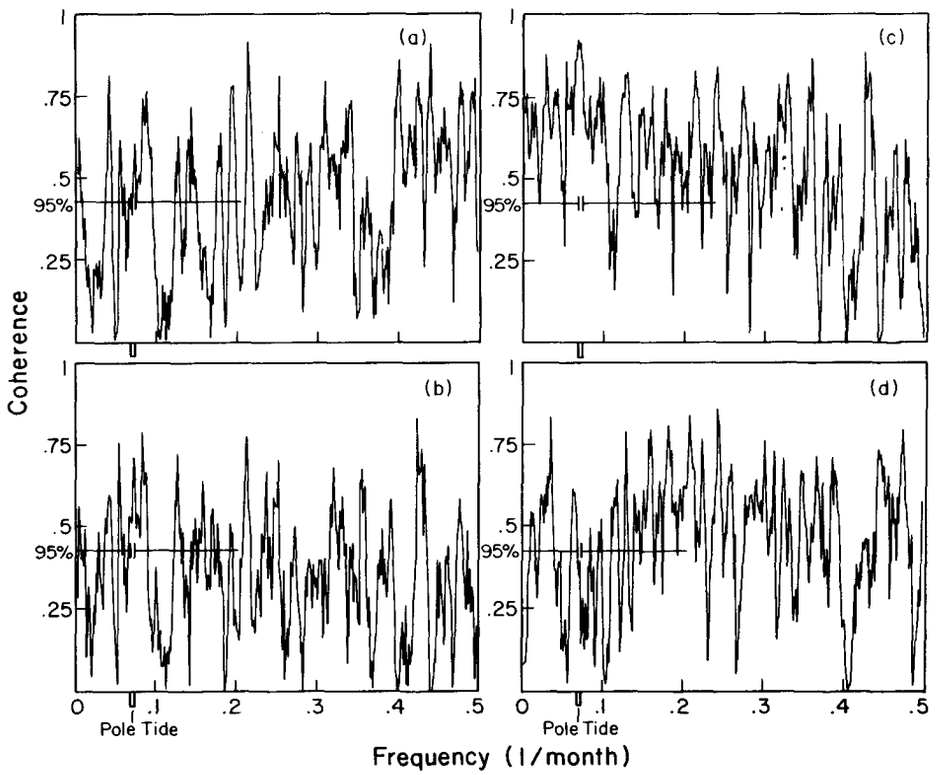

Figure 4. Coherence spectra for sea level versus pressure for Y_2^1 stacks of: (a) 26 North Sea stations; (b) 42 Baltic Sea stations; (c) 19 stations in Gulf of Bothnia; (d) 487 stations for global oceans outside the North Sea region. In all four parts of this figure, seasonal averages have been removed from sea level and pressure prior to constructing the coherence. There are several frequency bands where the coherence exceeds 0.43 (the 95 per cent confidence level), including the pole tide frequency band for the three shallow basins.

the atmosphere this region with a period of 14 months. The F-test exceeds the 90 per cent confidence level in several other frequency bands as well.

We are not suggesting that this is evidence of a pole tide in the atmosphere. In fact, the 14-month pressure peak is not a unique feature of the pressure spectrum [see Fig. 5(c), where the 14-month peak for pressure does not stand out among the other peaks].

To test for the existence of a resonance response of the shallow basins, the sea level data for each basin are fit in the frequency domain to resonant pressure and polar motion responses. For example, let $y(\omega)$ be the Fourier transform of the stacked data. Since wind data are not included here, we attempt to account for the wind-driven response by assuming it is proportional to the response to pressure. Then, we parametrize $y(\omega)$ using

$$y(\omega) = Ap(\omega) + Br(\omega) + \frac{Cp(\omega)}{\omega - \omega_0} + \frac{Dr(\omega)}{\omega - \omega_0} + \varepsilon(\omega). \qquad (7)$$

Here, A and B are the factors that describe the static response to pressure and winds and to the polar motion forcing, respectively [$p(\omega)$ and $r(\omega)$ are the Fourier transforms of the pressure and equilibrium pole tide]; C and D represent the resonant strengths for the meteorological forcing and the pole tide; ω_0 is the proposed resonance frequency in the basin; and $\varepsilon(\omega)$ represents unmodelled effects, including noise. If the observed peak in the basin near the pole tide frequency band is due to wind forcing which is correlated with pressure, then C and D will be small, and $y(\omega)$ will be dominated by the static terms. If the observed peaks are due to a resonance, then C and D will not be small, and ω_0 should, presumably, be close to the Chandler wobble frequency.

First, we find the values of A, B, C, D, and ω_0 that minimize $\varepsilon(\omega)$ in a least-squares sense. The inversion for ω_0 is non-linear, and so our procedure is to choose a great many values for ω_0 near the pole tide frequency, and fit for A, B, C, and D for each of these ω_0. We then look for an ω_0 which leads to a particularly pronounced decrease in the residuals. For all three basins, there are, indeed, pronounced reductions of the residuals when ω_0 is near the 437-day peak in the pole tide band. But, we judge the results to be inconclusive, due to the high correlation between the two resonant terms and $Br(\omega)$; when ω_0 is close to the pole tide period, it is difficult to separate the resonant term from the equilibrium tide.

Our second method of using (7) to test whether the data require an oceanic resonance, is to simultaneously fit and remove from the PSMSL stacks the non-resonant pressure and equilibrium pole tide [the terms proportional to A and B in (7)]. We band-pass the data to extract the pole tide band, prior to the fit. Results from the fits suggest that the pole tide in these shallow seas is much closer to equilibrium than is suggested by simply comparing sea level with the equilibrium tidal amplitude. For example, the results of the North Sea fit imply that the pole tide has an amplitude of 1.2 ± 1.2 times the equilibrium amplitude, and that the response to meteorology is 2.5 ± 1.3 times the inverted barometer pressure. For the Baltic Sea, the fit to the equilibrium pole tide is 1.9 ± 2.1 and the fit to pressure is 5.4 ± 1.8. For the Gulf of Bothnia the fitted parameters are 1.7 ± 1.0 and 4.5 ± 0.4. These large formal errors on the fits are the direct result of large variances of small numbers of data points. The pole tide frequency band encompasses only five elementary bandwidths, hence the two-way fit has only three degrees of freedom. Note that none of the pole tide parameters is significantly different from unity. For any of these three basins, if the fitted pressure and pole tide are removed from the PSMSL stack, the spectrum of the residuals (not shown) exhibits none of the characteristics of the equilibrium pole tide spectrum.

To help assess how strongly the data require a pole tide amplitude greater than the equilibrium amplitude, we subtract the equilibrium pole tide from the data [parameter B in (7) is constrained to be unity], and then fit and remove the pressure (parameter A, alone) from the PSMSL stack. If the spectrum of the residuals show the characteristic double peak of the pole tide spectrum, then there is reason to suspect an amplified response. If not, then the fact that the amplitude of B exceeded unity in the previous fit may be attributed to noise leaking into that fit.

Figures 5(a) and (b) show amplitude spectra of Y_2^1 stacks for the Baltic Sea and the Gulf of Bothnia. The sold line in each figure is the PSMSL data. The spectra of the PSMSL stack with pressure fitted and removed are the short dashed curves in Fig. 5(a) and (b). The long-dashed curves are the spectra of the residuals after subtracting the equilibrium pole tide (dash–dot curve) and fitting and removing pressure from the PSMSL stack. The spectra show that the removal of non-resonant pressure removes the majority of the enhanced power at the pole tide frequency. The spectra of the residuals after subtracting the equilibrium pole tide and then fitting and removing pressure have a double peak but they do not follow the characteristic peaks of the equilibrium pole tide closely. The North Sea results (not shown) are similar.

The problems brought about by the lack of wind data in this analysis are illustrated in Fig. 5(c) which shows power spectra of Y_2^1 stacks of pressure (the dashed line) and PSMSL data (the solid line) over the Baltic Sea for a wide frequency band. The peak at the pole tide frequency in the pressure spectrum is evident, but it is not appreciably larger than other pressure peaks. On the other hand, the peak in the pole tide band for the PSMSL data does stand above other peaks in this red spectrum. We can also infer there is something unusual happening in the pole tide band from the least-squares fit coefficients given above. For example, we have seen that the fit to pressure for the Baltic Sea gives 5.4 ± 1.8 across the pole tide band alone, but that it gives 1.2 ± 0.1 if the data are not band-passed prior to the fit.

Why is there such a large peak in sea level but not in pressure at the pole tide frequency? There are several possible explanations. It could be that there is a broad oceanic resonance across this band that amplifies the response to the meteorology. Perhaps the wind forcing, but not the pressure, is especially large in this frequency band. Or, maybe the wind is more highly correlated with pressure in this band, so that the wind-driven and pressure-driven responses tend to add constructively.

We conclude that, overall, our results are most consistent with the hypothesis that meteorological forcing near the pole tide frequency is responsible for most of the spectral peak in sea level at 434–437 days. We emphasize that the

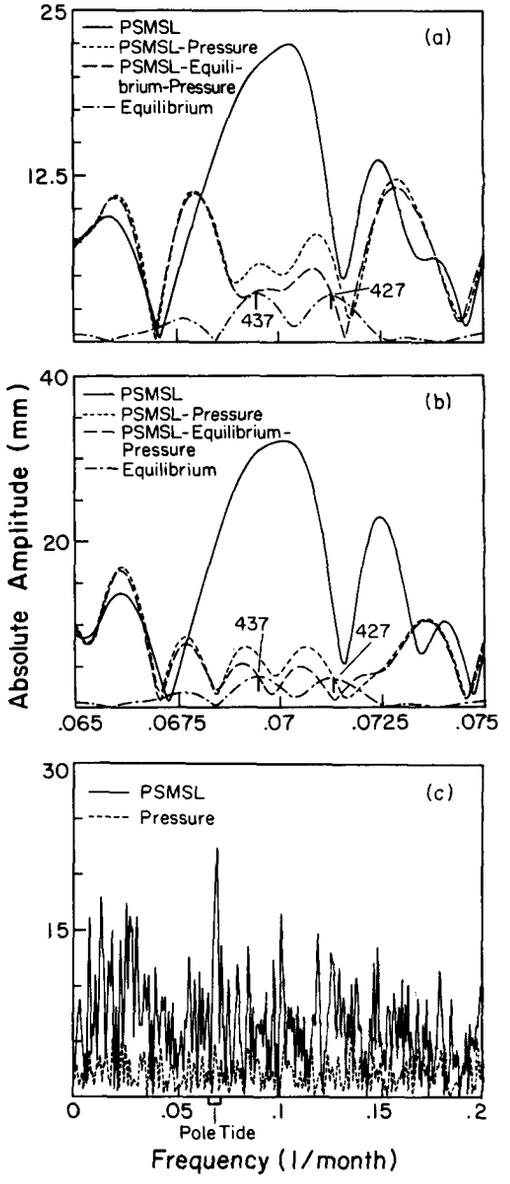

Figure 5. Amplitude spectra for Y_2^1 stacks from stations in the North Sea region. (a) Stacks for 42 stations in the Baltic Sea. The solid curve is PSMSL. The pressure is fitted and removed from the PSMSL data, giving the short-dashed curve. The equilibrium tide is removed and the pressure is fitted and removed to give the long-dashed curve. Note that the long-dashed curve does not follow the features of the equilibrium pole tide, which is the dash–dot curve near the bottom. (b) Same as (a), but for the 19 stations in the Gulf of Bothnia. (c) Stacks for the Baltic Sea, shown over a large frequency range. The solid curve is the PSMSL data, and the short-dashed curve is the pressure. Both spectra show peaks in the pole tide band, but the PSMSL peak stands above all other spectral peaks, the pressure peak does not.

PSMSL data that lie in the North Sea region are limited to the basin perimeters and have small numbers of stations, that we did not examine wind data, and that the frequency band of interest is narrow. We are, thus, not willing to conclusively rule out resonance as a mechanism for the enhanced spectral peak in these basins.

The 18.6-yr tide

Yearly tide gauge data are stacked against the equilibrium 18.6-yr tide for all 260 stations outside the Baltic Sea that reported at least 19 yr of data. The Baltic Sea is the only geographic area where long-period noise (there is a spectral peak at 22–23 yr in the Baltic Sea) so seriously masks the 18.6-yr signal as to affect the estimated phase of a global stack. We identify the Baltic Sea as a particularly noisy region as follows. First, annual and 18.6-yr amplitudes are fitted and removed from the data. Then, the standard deviation for the stacked data set is calculated, and we obtain $\sigma = 39.5$ mm. The majority of stations with outliers greater than 3σ are located in the Baltic Sea. The σ for the all stations outside the Baltic Sea is 34.8 mm. Data outliers are not removed from any of the 260 stations outside the Baltic Sea, as they do not affect the results for either the pole tide or the 18.6-yr tide enough to justify subjectively altering the data by their removal.

Figure 6 shows PSMSL and synthetic stacks against the equilibrium $\zeta(\theta, \lambda)$ in the time domain. A variation of approximately 16–20 yr may be seen in the PSMSL stack. Fig. 7(a) shows the amplitude spectra of ungridded equilibrium stacks. An 18.6-yr peak stands out clearly above the noise in the PSMSL data, and has an amplitude 1.2 times the synthetic amplitude. The PSMSL results also show pronounced peaks at 13.3- and 11-yr periods. The spectrum of the difference between the synthetic and PSMSL data shows that most of the discrepancy between the PSMSL and synthetic data at the 18.6-yr period may be attributed to noise, as the amplitude at the 18.6-yr period is well below the noise continuum. The results suggest that the PSMSL and synthetic data agree well in both amplitude and phase at the 18.6-yr period. Amplitude spectra for a stack against the equilibrium $\zeta(\theta, \lambda)$ on a $15° \times 30°$ grid is shown in Fig. 7(b). The use of a coarse grid improves the agreement between the PSMSL and synthetic amplitude at 18.6 yr.

A statistical F-test of the multitaper spectrum of the unweighted, ungridded data is shown in Fig. 8. (The multitaper spectrum, itself, is not shown here. It gives results similar to those shown in Fig. 7.) The F-test shows that we can be 95 per cent confident that the 18.6-yr signal

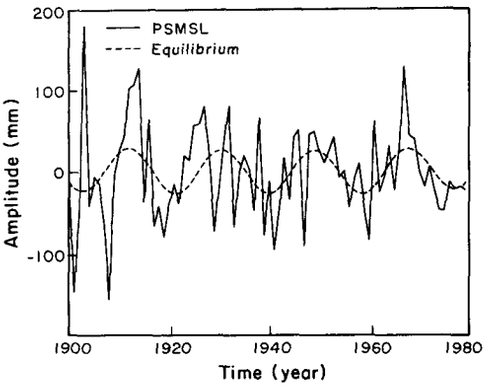

Figure 6. An ungridded Y_2^0 stack of 260 stations as a function of time. The 16–20-yr variation in the PSMSL stack, solid curve, is discernible, as is increased noise early in the time span. The dashed curve is the stack of synthetic data.

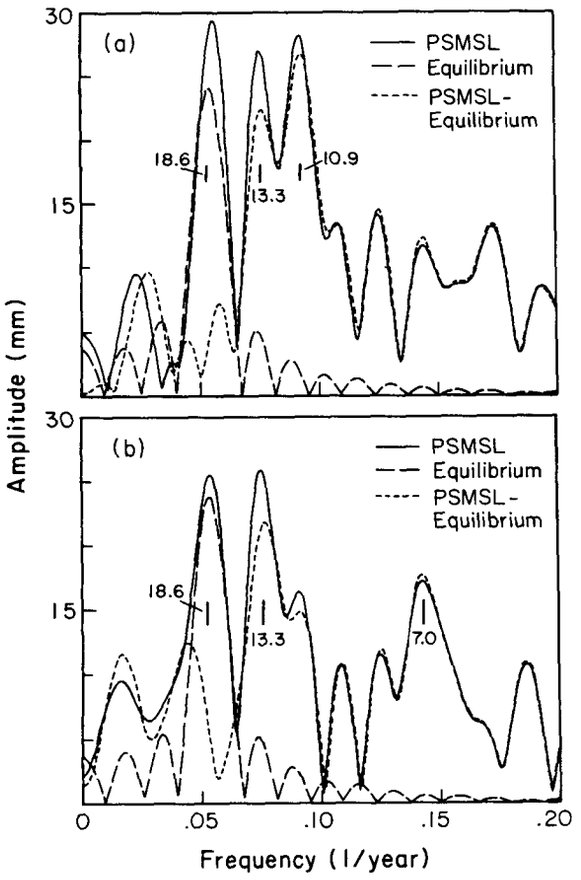

Figure 7. Amplitude spectra for Y_2^0 stacks of 260 stations outside the Baltic sea. The solid curve is the spectrum for the PSMSL data, the long-dashed curve is for the synthetic stack, and the short-dashed curve is a spectrum of the difference between the two stacks. (a) Ungridded. (b) 15° × 30° grid.

of the PSMSL data is sinusoidal. Note that the 13.3- and 11-yr peaks are not as prominent in the *F*-test results.

The phase of the difference between the time series is found by fitting an 18.6-yr sinusoid to both the PSMSL and the synthetic signals and comparing their phases. The uncertainty for the amplitude is estimated as described above for the pole tide results, and is calculated here using

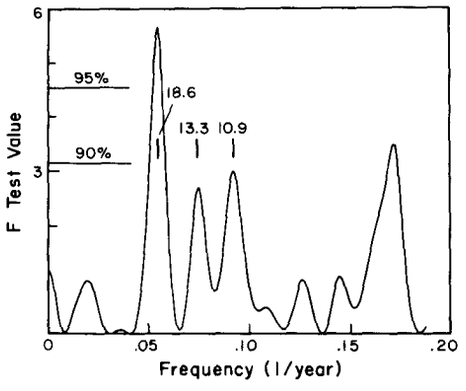

Figure 8. *F*-test derived from multitaper spectra for an ungridded Y_2^0 stack of the PSMSL signal. The *F*-test predicts with a 95 per cent certainty that the 18.6-yr peak is sinusoidal.

an estimated noise level of 5 mm for both the gridded and ungridded stacks. The results are as follows.

Ungridded PSMSL is 1.18 ± 0.22 times the synthetic; PSMSL leads by $1° \pm 30°$.

Gridded PSMSL is 1.07 ± 0.22 times the synthetic; PSMSL lags by $10° \pm 30°$.

We combine these results to estimate an amplitude for the 18.6-yr tide of 1.13 ± 0.22 times the equilibrium tide, and the phase of the tide to be equal to the equilibrium phase within a 30° uncertainty. A 30° phase difference corresponds to a time lead or lag of 19 months.

The agreement between the PSMSL and synthetic 18.6-yr spectral peaks is not overly sensitive to the removal of blocks of stations (with the exception of the Baltic Sea stations, which have already been removed) or to the use of time spans different from 1900 to 1979. For example, when all stations in other inland seas are removed from the data set, the amplitude at 18.6 yr is found to be affected by an amount that is within the range of the quoted uncertainties, although the frequency content of the noise does change.

The global rise in sea level

An observed secular sea level change at an individual station is not, by itself, evidence of a global rise in sea level. There could also be secular variations due to post-glacial rebound, local tectonic motion, or a shift in the wind-driven oceanic circulation pattern. The effects of these additional secular changes should be reduced in averages of global data. It is difficult, though, to adequately remove the effects of post-glacial rebound by averaging alone (Peltier 1986). Apparent changes in sea level at individual stations due to post-glacial rebound can be as large as 8.5 mm yr^{-1}, as is the case in the Gulf of Bothnia. Also, a disproportionately large percentage of tide gauges are in the northern hemisphere, close to the centres of rebound. Large numbers of stations also lie in tectonically active areas, and no reliable model exists that allows us to remove the crustal motion from all these stations.

We digitized the rebound results from Peltier's (1986) post-glacial rebound models for North America and northern Europe, and from Wagner & McAdoo (1986) for the remainder of the globe. In order to assess global sea level changes most accurately, we simultaneously fit the entire data set to a linear trend and to a synthetic data set consisting of a set of trends predicted for each station by the combined rebound models as described above.

In order to establish a uniform benchmark for each station, a line is fit to each station and the *y*-intercept of this line is subtracted from each station record before the simultaneous fit. The intercepts subtracted from each record in this way are not the true intercepts for those stations having less than 80 yr of data. For those subsets of stations containing many short records, this introduces a systematic error into the final trend. For example, if a station record having only a few years of data contains power at periods greater than the record length, the truncated periodic signals are correlated with the secular variability, and any true secular trend over several decades could be masked or even reversed.

On the other hand, if we restrict the data set to only those

stations having 80 yr or more of data, there might not be enough stations to optimally average out the secular variability caused by sources other than the global sea level rise. To compromise, we first construct a subset of the data that includes all stations with at least N years of data, where N is greater than 1 but probably less than 80. We choose N so that when we simultaneously fit the rebound and sea level rise to the data, the post-glacial rebound fit parameter is close to 1.

For an initial data set, we choose $N = 37$. This leaves us with 120 stations, and the simultaneous fit results in a rebound coefficient of 0.9. The increase in sea level revealed by the fit is 1.2 ± 0.1 mm yr^{-1}. The uncertainty is the rms value of the time series of global, yearly averages of all 120 stations, after the rebound is removed. A post-glacial coefficient of 0.9 is a good indication both that the post-glacial models are giving reasonable results, and that the global tide gauge data are capable of resolving linear trends on the order of mm per year.

In fact, we have been able to improve the fit by further restricting our global data set. First, we exclude 23 additional stations from regions of the globe having significant tectonic activity (all stations on the west coast of North America and Japan). When the 97 remaining stations in this reduced data set are simultaneously fit to the rebound data and the global sea level rise, the rebound coefficient is 0.94 and the rise in sea level is 1.6 ± 0.12 mm yr^{-1}.

We further exclude all stations south of 30°-N latitude. The post-glacial rebound in this area is small and is reasonably the same everywhere (and so it is not easily separable from a global rise in sea level), and is strongly dependent on assumptions about the Pleistocene deglaciation of Antarctica. This final data set consists of 84 stations, all with at least 37 yr of data, situated north of 30°-N latitude and away from Japan and the west coast of North America. The post-glacial rebound data for all these stations are estimated from the results of Peltier's (1986) model. For these stations, the fit to the rebound model is especially good at 0.994 and the fit to the linear trend is 1.75 ± 0.13 mm yr^{-1} over the last 80 yr. This trend is shown in Fig. 9.

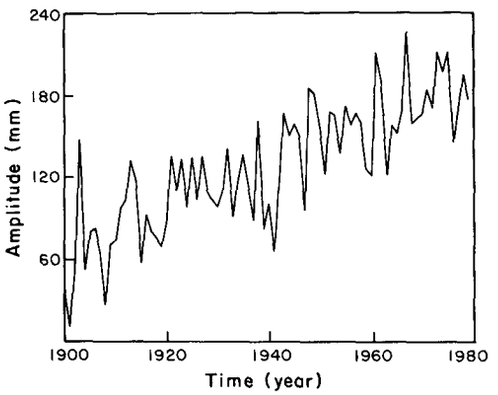

Figure 9. Linear trend for sea level for 84 stations having greater than 37 yr of data that lie north of 30°-N latitude and are not in tectonically active areas (Japan and the west coast of North America are excluded). Vertical motion at the surface is sumultaneously fit to these data using a model of post-glacial rebound from Peltier (1986). The fit to this model is excellent for these stations at 0.994, and the fitted rate of global increase in sea level is 1.75 ± 0.13 mm yr^{-1}.

From these three results, we estimate a global sea level rise during the last 8 decades of between 1.1 and 1.9 mm yr^{-1}, with a preferred value near 1.75 mm yr^{-1}. And, because the post-glacial fit parameter is so close to 1, we tentatively conclude that the effects of post-glacial rebound are well described by current models, and that the tide gauge data are capable of resolving global linear trends at the mm per year level.

CONCLUSIONS

By stacking global tide gauge data, we can significantly improve the signal-to-noise ratio for long-period tides, compared with results obtained from single-station records. We find that the 18.6-yr tide and the pole tide are clearly evident above the noise in the spectra for the equilibrium stacks. The peaks are not evident in stacks against other pure spherical harmonics. The observed amplitude and phase for the 18.6-yr tide are consistent with the assumption of global equilibrium. The amplitude and phase of the pole tide are close to the equilibrium amplitude and phase for all regions outside the North Sea, Baltic Sea and Gulf of Bothnia. In these basins, the enhanced tide appears to be more consistent with narrow band meteorological forcing centred about the pole tide frequency than to a resonant response of the oceanic basin, although the results are not entirely conclusive. We find that in all regions except the Baltic Sea and Gulf of Bothnia, the oceanic response to atmospheric pressure is consistent with inverted barometer hypothesis for periods longer than 2 months. Our conclusions are based on the assumption that by using many stations, we were able to break the correlation between winds and pressure. This cannot be confirmed without including wind data in our analysis.

Finally, by simultaneously fitting the global sea level data to a linear trend and data prepared from a combined post-glacial rebound model, we conclude that the global rise in sea level over the last several decades was between 1.1 and 1.9 mm yr^{-1}, with a preferred value near 1.75 mm yr^{-1}. Furthermore, the good agreement with the results from the post-glacial models suggests that those results are reasonably representative of the true uplift, and that the tide gauge data are capable of resolving global changes in sea level at the mm per year level.

ACKNOWLEDGMENTS

We are grateful to Neamen Tewahade for his help in digitizing and interpolating the post-glacial rebound results, and to Carl Wunsch for providing valuable comments on the manuscript. We thank the Permanent Service for Mean Sea Level for providing us with the tide gauge data. This work was supported in part by NASA (grant NAGS-485) and the Air Force Geophysical Laboratory (contract F19628-86-k-0011).

REFERENCES

Barnett, T. P., 1983. Possible changes in global sea level and their causes, *Climate Change*, **5**, 15–38.

Carton, J. A. & Wahr, J. M., 1986. Modelling the pole tide and its effect on the Earth's rotation, *Geophys. J. R. astr. Soc.*, **84,** 121–138.

Cartwright, D. E. & Tayler, R. J., 1971. New computations of the tide-generating potential, *Geophys. J. R. astr. Soc.*, **23,** 45–74.

Cartwright, D. E. & Edden, A. C., 1973. Corrected tables of tidal harmonics, *Geophys. J. R. astr. Soc.*, **33,** 253–264.

Chao, B. F., 1988. Correlation of interannual length-of-day variation with El Nino/southern oscillation, 1972–1986, *J. geophys. Res.*, **93,** B7,7709-7715.

Chelton, D. & Enfield, D., 1986. Ocean signals in tide gauge records, *J. geophys. Res.*, **91,** 9081–9098.

Dahlen, F. A., 1976. The passive influence of the oceans on the rotation of the Earth, *Geophys. J. R. astr. Soc.*, **46,** 363–406.

Dickman, S. R., 1988a. The self-consistent dynamic pole tide in non-global oceans, *Geophys. J.*, **94,** 519–543.

Dickman, S. R., 1988b. Theoretical investigation of the oceanic inverted barometer response, *J. geophys. Res.*, **93,** 14 941–14 946.

Emery, K. O., 1980. Relative sea level from tide-gauge records, *Proc. nat. Acad. Sci.*, **77,** 6968–6972.

Gilbert, F. & Dziewonski, A. M., 1975. An application of normal mode theory to the retrieval of structural parameters and source mechanisms from seismic spectra, *Phil. Trans. R. Soc. Lond. A*, **278,** 187–269.

Gornitz, V., Lebedeff, S. & Hansen, J., 1982. Global sea level trend in the past century, *Science*, **215,** 1611–1614.

Hansen, J., Johnson, D., Lacis, A., Lebedeff, S., Lee, P., Rind, D. & Russel, G., 1981. Climate impact of increasing atmospheric carbon dioxide, *Science*, **213,** 957–966.

Hosoyama, K., Naito, I. & Sato, N., 1976. Tidal admittance of pole tide, *J. Phys. Earth*, **24,** 51–62.

Lambeck, K. & Nakiboglu, S. M., 1983. *Geophys. Res. Lett.*, **10,** 857–860.

Lindberg, C. R., Park, J. & Thomson, D. J., 1987. Multiple taper analysis of terrestrial free oscillations, parts I and II, *Geophys. J. R. astr. Soc.*, **91,** 755–836.

Luther, D. S., 1982. Evidence of a 4–6 day barotropic, planetary oscillation of the Pacific Ocean, *J. Phys. Ocean.*, **12,** 644–657.

Merriam, J. B., 1982. Meteorological excitation of the annual polar motion, *Geophys. J. R. astr. Soc.*, **70,** 41–56.

Miller, S. P. & Wunsch, C., 1973. The pole tide, *Nature Phys. Sci.*, **246,** 98–102.

Munk, W. H. & Hassan, E. M., 1961. Atmospheric excitation of the earth's wobble, *Geophys. J. R. astr. Soc.*, **4,** 339–358.

Munk, W. H. & Cartwright, D. E., 1966. Tidal spectroscopy and prediction, *Phil. Trans. R. Soc. Lond. A*, **259,** 533–581.

Munk, W. H. & Macdonald, G. J. F., 1975. *The Rotation of the Earth,* Appendix, Cambridge University Press, Cambridge, UK.

O'Connor, W. P., 1986. The 14-month wind stressed residual circulation (pole tide) in the North Sea, *NASA Technical Memorandum 87800.*

O'Connor, W. P. & Starr, T. B., 1983. Approximate particular solutions for the pole tide in a global ocean, *Geophys. J. R. astr. Soc.*, **75,** 397–405.

Peltier, W. R., 1986. Deglaciation-induced vertical motion of the North American Continent and transient lower mantle rheology, *J. geophys. Res.*, **91,** B9,9099–9123.

Pugh, D. T. & Faull, H. E., 1983a. *Monthly and Annual Mean Heights of Sea Level, Permanent Service for Mean Sea-Level,* Institute of Oceanographic Sciences, Bidston Observatory, Birkenhead, Merseyside, UK.

Pugh, D. T. & Faull, H. E., 1983b. Operational sea-level stations, *Intergovernmental Oceanographic Commission Technical Series, 23,* Institute of Oceanographic Sciences, Bidston Observatory, Birkenhead, Merseyside, UK.

Rabbel, W. & Zschau, J., 1985. Static deformation and gravity changes at the earth's surface due to atmospheric loading, *J. Geophys.*, **56,** 81–99.

Rubincam, D. P., 1984. Post glacial rebound observed by Lageos and the effective viscosity of the lower mantle, *J. geophys. Res.*, **89,** 1077–1088.

Smith, M. L. & Dahlen, F. A., 1981. The period and Q of the Chandler wobble, *Geophys. J. R. astr. Soc.*, **64,** 223–282.

Thomson, D. J., 1982. Spectrum estimation and harmonic analysis. *Proc. IEEE*, **70,** 9, 1055–1096.

Van Dam, T. & Wahr, J. M., 1987. Displacements of the earth's surface due to atmospheric loading: effects on gravity and baseline measurements, *J. geophys. Res.*, **92,** 1281–1286.

Wagner, C. A. & McAdoo, D. C., 1986. Time variations in the Earth's gravity field detectable with geopotential research mission intersatellite tracking, *J. geophys. Res.*, **91,** B8, 8373–8386.

Wahr, J. M., 1983. The effects of the atmosphere and oceans on the earth's wobble and on the seasonal variations in the length of day-2. Results, *Geophys. J. R. astr. Soc.*, **74,** 451–487.

Wilson, C. R. & Haubrich, R., 1976. Meteorological excitation of the earth's wobble, *Geophys. J. R. astr. Soc.*, **46,** 707–743.

Wunsch, C., 1972. Bermuda sea level in relation to tides, weather, and baroclinic fluctuations, *Rev. Geophys. Space Phys.*, **10,** 1–49.

Wunsch, C., 1986. Dynamics of the North Sea pole tide reconsidered, *Geophys. J. R. astr. Soc.*, **87,** 869–884.

Yumi, S. & Yokoyama, K., 1980. *Results of the International Latitude Service In a Homogeneous System,* Central Bureau of The International Polar Motion Service, International Latitude Observatory of Mizusawa, Mizusawa, Japan.